Developing a parametric system model to describe the product distribution of steam pyrolysis in a Dual Fluidized bed

(article starts on next page)

Full Length Article

Developing a parametric system model to describe the product distribution of steam pyrolysis in a Dual Fluidized bed

Renesteban Forero-Franco [*], Teresa Berdugo-Vilches, Chahat Mandviwala, Martin Seemann, Henrik Thunman

Department of Space, Earth and Environment (SEE), Division of Energy Technology, Chalmers University of Technology, 41296 Gothenburg, Sweden

A B S T R A C T

Steam pyrolysis is a thermochemical process that converts carbon-based materials into valuable gases. In general, the products of the reaction are syngas (H_2, CO, CO_2), low-molecular-weight hydrocarbon gases (methane, ethylene, and propylene), pyrolytic gasoline and oils, monoaromatic and polyaromatic species (tar), and carbonaceous residues (char) with ashes. However, the intricacy of the reactions comprising the process, the diversity of the product species, and the constraints linked to the sampling and measurement equipment, create a highly complex system. In this work, a method for data representation is presented based on a special Parametric System Model (PSM) that portrays product species measurements in a way that provides relevant information and valuable insights into the process. The method incorporates generic knowledge of the chemical nature of the reactions to create a constrained system in which the data can be expressed in parametric terms with meaningful statistical functions. The evaluated data were obtained from a high-temperature steam pyrolysis process performed in the 2–4-MW Dual Fluidized Bed reactor at Chalmers University using polyethylene as feedstock. The quantities of the hydrocarbon species detected in the gas product were taken for the PSM as a probabilistic system that can be described with a set of distribution functions. The carbon, hydrogen and oxygen balances were taken into account to build a constrained set of equations to find the parameters of the functions. The resulting model was proven to be useful as a prediction tool to quantify unmeasured carbon group species and to estimate process variables, such as the oxygen transport of the bed material. Also, it was demonstrated the potential of the model as a method to identify and estimate inconsistencies in the measurements, which improve the quality of the characterization data. The model̇s outcomes find application in providing critical information for the control and evaluation of pyrolysis process and downstream operation of biorefineries.

1. Introduction

In the high-temperature steam pyrolysis process, conversion of a carbon feedstock takes place in the presence of steam, which acts as a dilution and almost inert agent, at relatively high temperatures (~800 °C). The endothermic conversion leads to the production of a combustible gas, called the "producer gas", which contains H_2, CO, CO_2 and hydrocarbons in the forms of paraffins, olefins and aromatics that can subsequently be used in further chemical or energy processes. This distribution of species in the producer gas is defined by the pyrolysis conditions and feedstock characteristics.

In general, pyrolysis reactions are endothermic in nature, which means that heat must be added to the reactor to cover the process energy demands. The reactor type and design exert an important influence on the gas product species distribution. Several types of reactors are currently in use in industry with different design and working principles [1]. Dual Fluidized Beds (DFBs) are notable for their heat transfer and mixing characteristics, providing robust transformation of different kinds of feedstocks. The DFB technology is used in this work. The fluidization conditions, and in particular the bed type, are among the most-relevant operational variables that have impacts on the contents of the pyrolysis products. In fact, depending on the molecular structure of the bed material and its oxygen transport characteristics, the chemical balances of the pyrolysis products align towards a certain component, thereby modifying its share.

Once the pyrolysis process is completed, the producer gas passes through a series of setups to clean it for further processing and characterization. The online species quantification can be performed in a gas

---

* Corresponding author.
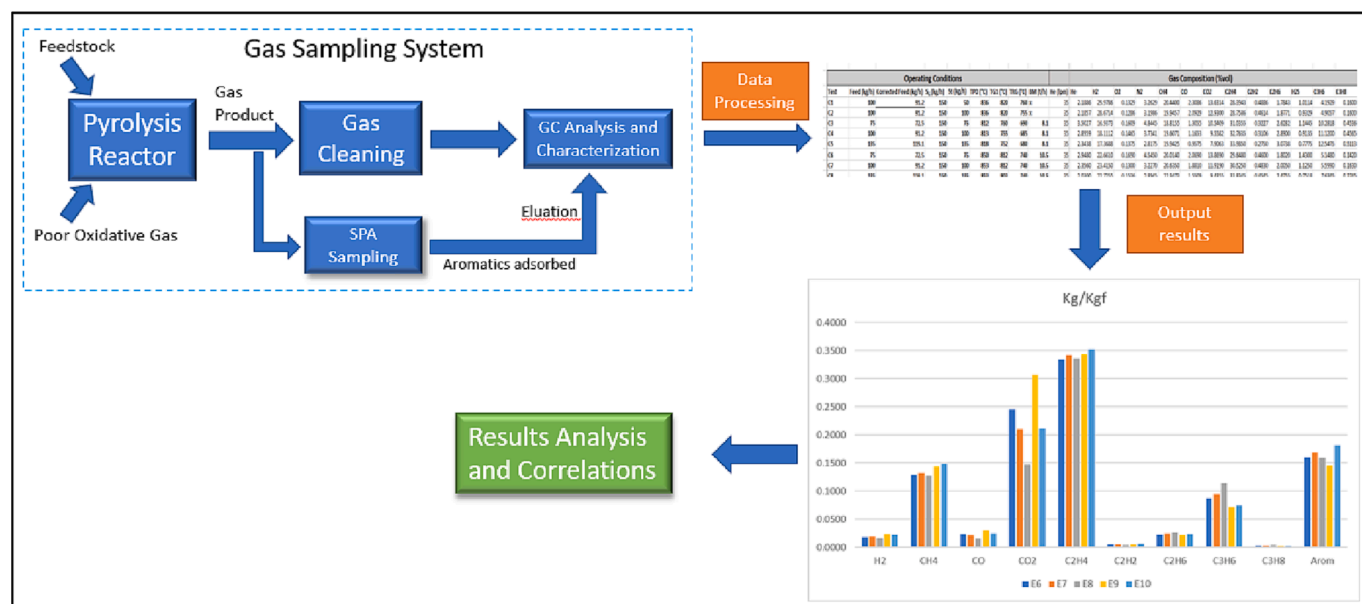*E-mail address:* rforero@chalmers.se (R. Forero-Franco).

Fig. 1. Example of a pathway for data collection and processing to get a "plain" graphical compilation of the species information. The gas sampling system schema depicts the one used in this work, but this can differ from one experimental setup to another.

chromatograph equipped with a species detector (see Section 3). The chromatographic results for the different species found in the producer gas are compiled as %v/v (based on calibration curves) and usually presented in tables, where the volume concentration is converted to, e. g., $moles/kg_{fuel}$ or %wt according to the fuel flow and internal or external standard methods. Following this tabulation, the results are graphically presented in sets of column bars for the relevant species obtained (Fig. 1).

Though very straightforward to display, this "plain" graphical representation of the results presents some challenges. First, the information is limited to the species that the analytical instrument can detect, so it cannot give information about the non-measured species to close the system's carbon balance. Second, when dealing with many different process conditions and feedstocks, numerous and large tables are usually produced and reported, entailing a difficult data mining task when trying to extract the relevant information even from a single case. Additionally, the lack of generic knowledge of the process nature in the plain graphical representation makes any inter-case study very limited and not very useful for behavior prediction or operational space exploration. Third, when progressing towards heterogeneous mixtures and wide variations in operational conditions, the source of the variation in the results is obscured. Thus, it becomes problematic to determine correlations between the response in the graph and the operational variables that were modified.

In general, three factors can be identified as the main sources of variation in the results: 1) changes in the feedstock; 2) changes in the thermodynamics of the operation; and 3) errors or constraints associated with the measurements from the setup used. These three sources are influential to greater or lesser degrees depending on the process evaluated and its operational conditions. In that sense, a representation of the data that allows to correlate any relevant changes in the measurements with these sources of variation must be implicitly connected to the nature of the process itself. Such a method must be capable of providing generic knowledge of the evaluated system, while facilitating comparisons between similar processes. To the best of our knowledge, this is something that has not been performed previously for pyrolysis processes. Therefore, this work constitutes an attempt to develop a model built on a special data representation method that can deal with the challenges of the plain data way and can provide broader and more-meaningful information regarding the process measurements.

For the purpose of this article, experimental data from steam pyrolysis in a DFB is here employed. To show the ability of the method to extract information of process variables, we focus on the example of estimating the Bed's Oxygen Transport (BOT) based on the method outputs.

The BOT is a phenomenon that occurs in DFB reactors when the bed material contains oxygen carrying species. In DFB reactors the circulating bed acts as a carrier medium that transports: heat from the combustor to the pyrolysis chamber; char from the pyrolyzer to the combustor; and active species between the combustor and the pyrolyzer. Regarding the latter, the bed material can contain, or transport from the combustor side, active components that interact with the feedstock in the pyrolyzer, thereby modifying its gas product composition. Silica sand is normally used as reference case due to its low chemical reactivity with the feedstock. Although silicate molecules can be considered virtually inert at the typical steam pyrolysis temperatures ($750^\circ C$), even traces of transition metal oxides, such as Fe_2O_3, can act as oxygen donors in the pyrolysis process [2]. Furthermore, ashes coming from the combustor side can be a source of oxygen in reducing environments as pointed out by Berdugo et al. [3]. For instance, ashes that contain calcium can participate in a redox cycle in the presence of sulphur. $CaSO_4$ transforms into CaS in the pyrolyzer's reducing environment, looping back to form $CaSO_4$ under the oxidative conditions in the combustor. These redox processes have been studied for Chemical Looping Cycle (CLC) systems [4], and are also relevant to other DFB applications.

The aim of this work is to develop a validated model that captures the product distribution of a pyrolysis process based on known mathematical distribution functions governed by chemical and statistical considerations. The model's framework will be defined by hard constraints such as elemental balances, functions' topology and convergence criteria. By creating a highly constrained system, the ultimate goal is to define a model that be able to get physical and mathematical consistent information about the chemical system that can lead to 1) validation of the results through data quality assessment, 2) estimation of hard-to-measure species and 3) establishment of a parametric function as a way to compress the information and potentially be used as a fingerprint of a particular process condition. Specifically, the focus here will be on presenting the development of the model and its validation. Additionally, the application of the model as a predictive tool is investigated to estimate unmeasured species as well as important process variables such
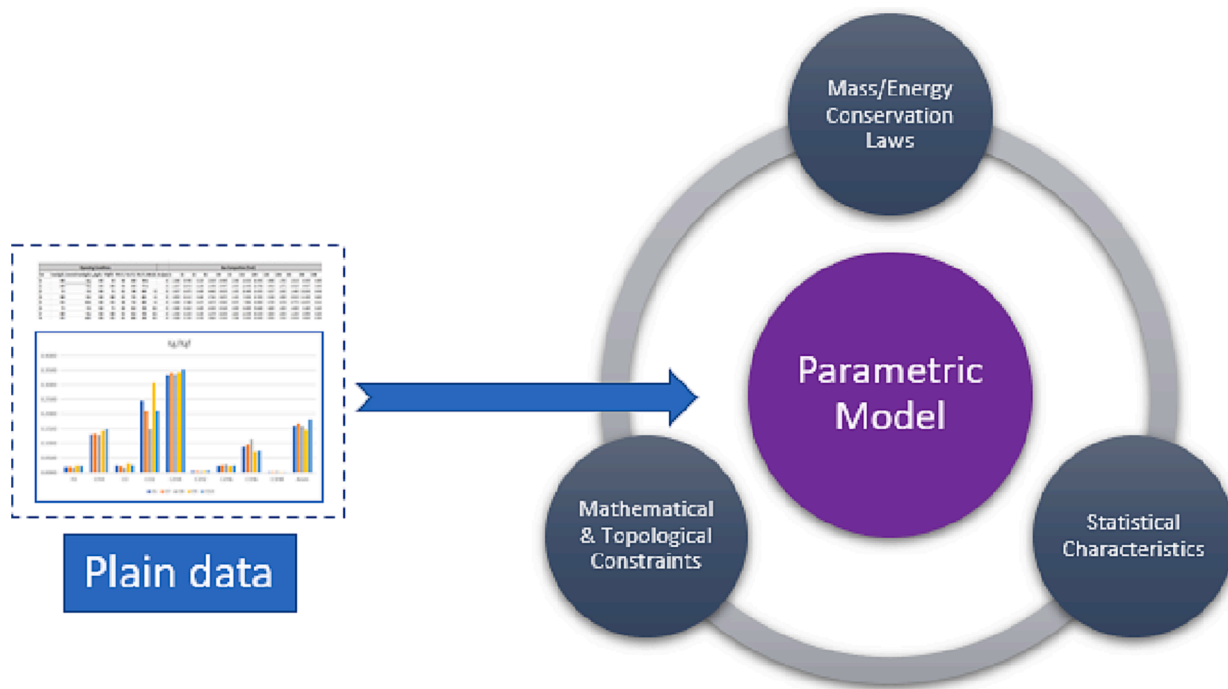
Fig. 2. Conceptual schema of the "plain data" transformation into the proposed parametric model.

as the BOT. Finally, the potential of the model to assess data quality and experimental error identification is explored by deliberately introducing a systematic error in the data set.

In the grand scheme of things, this study lays the chemical and mathematical foundations of a parametric model that can be utilized as a tool for the operation and control of pyrolysis process plants.

2. Model description

2.1. Theoretical framework

The method consists of introducing the measured data into a Parametric System Model (PSM), which is enclosed in a framework governed by certain chemical and statistical characteristics of the pyrolytic conversion process. The model's kernel is a set of mathematical functions with characteristic topologies, which introduce additional constraints to the framework (see Fig. 2). Within its formulation, the final constrained system will contain global knowledge about the process that incorporates not only the measured data, but also the unknown data. This provides possibilities to: perform estimations of important unknown quantities that could not be measured due to equipment constraints; identify inconsistencies in the measured data; and rank certain measurements according to relevance for the system in terms of accuracy improvements and setting minimum values for the sampling characterization effort.

In practice, it was observed that the results from the measured species could be separated into four groups: Paraffins, Olefins, Aromatics, and Syngas. These groups represent different molecular systems based on which the original feedstock is converted. They are also governed by mass and energy conservation laws, which represent the main constraints on the model framework. In our case, only the mass conservation is considered and expressed in terms of the elemental balances of the system. In particular, for a steam pyrolysis process and a fuel based on carbon, hydrogen and oxygen (C, H, O), Equations (1)–(3) are obtained:

$$\sum_{k=1}^{\infty} n_{C,k}^{pf} + \sum_{k=1}^{\infty} n_{C,k}^{of} + n_C^{arom} + n_C^{CO} + n_C^{CO_2} + n_C^{char_{out}} = n_C^{fuel} + n_C^{char_{in}} \quad (1)$$

$$\sum_{k=1}^{\infty} n_{H,k}^{pf} + \sum_{k=1}^{\infty} \sum_{l} n_{H,k,l}^{of} + n_{H,total}^{arom} + n_H^{H_2,out} + n_H^{H_2O,out}$$
$$= n_H^{fuel} + n_H^{H_2,in} + n_H^{H_2O,in} \quad (2)$$

$$n_O^{CO} + n_O^{CO_2} + n_O^{HC,out} + n_O^{H_2O,out} + n_O^{O_2,out} = n_O^{fuel} + n_O^{H_2O,in} + n_O^{O_2,in} \quad (3)$$

Here, $n_{a,k}$ corresponds to the moles of a particular chemical element ($a \in$ {C, H, O}), and the superscript indicates the evaluated molecule or system (*pf* and *of* indicate paraffins and olefins, respectively). The term k represents the number of carbons that a particular paraffin or olefin chain contains, referred to hereinafter as the carbon group (or just the *k*-group). In Equation (2), *l* covers all possible olefin species of a particular *k*-group. In Equation (3), $n_O^{HC,out}$ corresponds to the moles of oxygen in the produced hydrocarbon species with oxygen atoms in their structures (for instance, some oxygenated aromatic species). The term $n_C^{char_{in}}$ accounts for external sources of char entering the system, for instance, char transported from the combustor side during the DFB cycle.

This mode of representation in terms of carbon groups or carbon number, known as the carbon number distribution, has been employed in the petrochemical industry to elucidate typical distributions of carbon species coming from refinery and cracking/pyrolysis processes [5–7] (the cited references depict this kind of distribution for thermal cracking of polyolefins and Fischer-Tropsch waxes, and use them to evaluate the general species distribution for different severity levels). This representation is normally brought up in research on pyrolysis decomposition when comparing the yields of certain organic species of a particular size, so as to evaluate the quality of the products from a particular pyrolysis process for liquid fuels [8,9]. For the purposes of the present study, the usefulness of this representation lies in the possibility to represent the mole quantities of the paraffins and olefins as mathematical sequences that can be summed over an infinite range of k-groups, as expressed in Equations (1)–(3). In reality, the polymers in a feedstock comprise hundreds of thousands of monomer units. Thus, relative to such high numbers of arranged carbon atoms, the limit to the infinite is simply a mathematical formality to avoid any restriction on the length of a species that can be formed from the process. These series must be convergent, which imposes certain behavioral rules for the sequences or the

Table 1

List of mono-parametric and bi-parametric distribution functions used in this work. The asterisk marked rows correspond with heavy-tailed distributions. (Con-Max, Conway-Maxwell Distribution; Gamma-Inv, Gamma Inverted Distribution).

Distribution's Name	Mathematical Expression
Geometric	$f_k(\alpha) = \alpha(1-\alpha)^{k-1}; 0 < \alpha < 1$
Flory-Schultz	$f_k(\alpha) = \alpha^2 k(1-\alpha)^{k-1}; 0 < \alpha < 1$
Poisson	$f_k(\alpha) = \alpha^{k-1} e^{-\alpha}/(k-1)!; \alpha > 0$
Neg. Binomial	$f_k(\alpha,\beta) = \Gamma(k+\beta-1)\alpha^r(1-\alpha)^{k-1}/(\Gamma(k)\Gamma(\beta)); \beta > 0, \alpha \in [0,1]$
Con-Max	$f_k(\alpha,\beta) = \alpha^{(k-1)}/\left(Z(\alpha,\beta)*((k-1)!)^\beta\right); \alpha,\beta > 0$
Burr *	$f_k(\alpha,\beta) = (1+(k-1)^\alpha)^{-\beta} - (1+k^\alpha)^{-\beta}; \alpha,\beta > 0$
Fréchet *	$f_k(\alpha,\beta) = e^{-(k/\alpha)^{-\beta}} - e^{-((k-1)/\alpha)^{-\beta}}; \alpha,\beta > 0$
Dagum *	$f_k(\alpha,\beta) = (1+k^{-\alpha})^{-\beta} - (1+(k-1)^{-\alpha})^{-\beta}; \alpha,\beta > 0$
Gompertz	$f_k(\alpha,\beta) = e^{-\alpha(e^{\beta(k-1)}-1)} - e^{-\alpha(e^{\beta k}-1)}; \alpha,\beta > 0$
Weibull *	$f_k(\alpha,\beta) = e^{-((k-1)/\alpha)^\beta} - e^{-(k/\alpha)^\beta}; \alpha,\beta > 0$
Gamma	$f_k(\alpha,\beta) = \gamma(\alpha,\beta(k-1))/\Gamma(\alpha) - \gamma(\alpha,\beta k)/\Gamma(\alpha); \alpha,\beta > 0$
Lomax *	$f_k(\alpha,\beta) = (1+(k-1)/\alpha)^{-\beta} - (1+k/\alpha)^{-\beta}; \alpha,\beta > 0$
Gamma_Inv *	$f_k(\alpha,\beta) = \gamma(\alpha,\beta/(k-1))/\Gamma(\alpha) - \gamma(\alpha,\beta/k)/\Gamma(\alpha); \alpha,\beta > 0$

functions associated with them.

Equations (1)–(3) can be rewritten in terms of molar fractions and the H/C mole ratio of each *k*-group to get the system of equations that define the PSM as a chemical system. By taking the number of moles $n_{C,k}$ as $n_{C,k} = n_{C,tot}X_{C,k}$, where n_C corresponds to the total moles of the paraffin or olefin system and $X_{C,k}$ is the molar fraction over all *k*, the final equations will be:

$$n_{C,tot}^{pf}\sum_{k=1}^{\infty}X_{C,k}^{pf} + n_{C,tot}^{of}\sum_{k=1}^{\infty}X_{C,k}^{of} + n_C^{arom} + n_C^{CO} + n_C^{char,out} = n_C^{fuel} + n_C^{char,in} \tag{4}$$

$$n_{C,tot}^{pf}\sum_{k=1}^{\infty}X_{C,k}^{pf}\gamma_k^{pf} + n_{C,tot}^{of}\sum_{k=1}^{\infty}X_{C,k}^{of}\gamma_{k,eff}^{of} + n_{H,total}^{arom} + n_H^{H_2,out} + n_H^{H_2O,out}$$
$$= n_H^{fuel} + n_H^{H_2O,in} + n_H^{H_2,in} \tag{5}$$

$$\gamma_k^{pf} = \left(2+\frac{2}{k}\right); \gamma_{k,eff}^{of} = \sum_{g=0}^{2\lfloor k/2\rfloor-1}X_{C,k,g}^{of}\left(2-\frac{2g}{k}\right) \tag{6}$$

The term, $\gamma_{k,eff}^{of}$, as defined in Equation (6), arises when simplifying the hydrogen equation by grouping together the olefin species depending on their chemical formulas (the expression $\lfloor x\rfloor$ indicates the greatest integer less than or equal to x). It can be regarded as the effective H/C ratio, given the different olefin species that can be found for each k-group. Thus, *g* corresponds to the olefin group of a particular k-group with $2(k-g)$ hydrogens. In other words, *g* is the number of hydrogen pairs that are missed from the mono-ene case ($g = 0$). For instance, taking $k = 4$ and $g = 1$ means that a four-carbon chain is evaluated that has one pair of H less than the butene case, i.e., a chain with molecular formula C_4H_6, which is a diene.

2.2. Parametric model definition

In most of the online sampling setups, the amounts of C1–C3 paraffin and olefin species are usually measured with relative ease. After C3, the number of species per *k*-group grows exponentially and with ever-lower amounts. This means that not only does it take more time to perform the analysis, but that also specialized and costly equipment are required, sometimes corresponding even with offline setups. This is one of the main reasons why it is uncommon to find reports in the literature describing the total amounts of C4 or higher *k*-groups. For the aromatics case, a reasonable number of species can be measured (from C6 to C14) using SPA analysis, which provides a good estimation of the total moles for this system, as presented by Israelsson et. Al. and Berdugo et. Al. in

references [10,11]. However, this is an offline method, since the aromatics must be extracted from the gas sampling line with an SPA syringe and thereafter eluated for analysis in a GC. Moreover, the SPA method can include some errors, as not all the measurable species are being adsorbed in the column, although this can be mitigated to some extent by using an adequate adsorption column [11].

From the carbon balance (Eq. (4), by definition, the sum over all *k* of $X_{C,k}^S$ must be equal to one ($S \in \{pf, of\}$). This molar fraction $X_{C,k}^S$ can be seen as a discrete probability function or, more precisely, a mass density function (mdf) for the evaluated molecular system. As explained previously, in practice, the full extent of the $X_{C,k}^S$ sequences are virtually unknown, so the model's core is to replace those infinite sequences with discrete probability functions that are defined based on a finite set of parameters.

In that sense, the unknown molar fractions of paraffins ($X_{C,k}^{pf}$) and olefins ($X_{C,k}^{of}$) in Equations (4) and (5) can be expressed as:

$$X_{C,k}^{pf} = f_{C,k}^{pf}\left(\alpha_1^{pf}, \alpha_2^{pf}, \cdots, \alpha_n^{pf}\right);$$
$$X_{C,k}^{of} = f_{C,k}^{of}\left(\alpha_1^{of}, \alpha_2^{of}, \cdots, \alpha_n^{of}\right) \tag{7}$$

$$X_{H,k}^{pf} = X_{C,k}^{pf}\gamma_k^{pf} = f_{H,k}^{pf}\left(\alpha_1^{pf}, \alpha_2^{pf}, \cdots, \alpha_n^{pf}\right);$$
$$X_{H,k}^{of} = X_{C,k}^{of}\gamma_{k,eff}^{of} = f_{H,k}^{of}\left(\beta_1^{of}, \beta_2^{of}, \cdots, \beta_m^{of}\right) \tag{8}$$

$$n_{a,tot}^{pf} = \frac{\sum_{k=1}^{K_{ms}^{pf}}n_{a,k}^{pf,ms}}{\sum_{k=1}^{K_{ms}^{pf}}f_{a,k}^{pf}}; n_{a,tot}^{of} = \frac{\sum_{k=2}^{K_{ms}^{of}}n_{a,k}^{of,ms}}{\sum_{k=2}^{K_{ms}^{of}}f_{a,k}^{of}} \tag{9}$$

where K_{ms}^{pf} and K_{ms}^{of} correspond to the maximum measured *k*-group for the paraffin and olefin species, respectively. The term $f_{a,k}^S$ is a discrete function with a semi-infinite support $k \in \{1, 2, 3\cdots\}$, which is defined with a finite set of shape parameters $\{\alpha_1, \cdots, \alpha_n\}$ or $\{\beta_1, \cdots, \beta_m\}$; $a \in \{C, H\}$ and $S \in \{pf, of\}$.

The advantages of this approach reside in that it can provide a closed form solution to the equation system formed by Equations (4) and (5), and at the same time it can deliver the topology and the convergence criteria needed to satisfy the model's mathematical constraints.

2.3. Model implementation

The more shape parameters that the function has, the more flexible it will be for highly skewed data. However, the goal is to define a function f_k that can be fitted to the measured data with the minimum number of shape parameters and give a good estimation of the unknown species according to the carbon and hydrogen balances. The search for a suitable function is not a simple task, owing to the characteristic form of the measured data in the pyrolysis processes, as well as to the stringent restrictions imposed on its mathematical definition and topology. In general, the function must satisfy the following conditions: 1) it must present a decaying behavior with the possibility of becoming a mono-modal and positively skewed function; 2) it must be sufficiently flexible to handle relatively large changes in the concentration of species while still fitting with the measured data; 3) it needs to be defined with the lowest number of parameters possible; and 4) the function's form and predicted area must be such that the conservation laws are satisfied. Further discussion on the function's topological conditions can be found in Section 7.1 of the Appendix.

Several types of functions are candidates for the test proving that they can fit with the results obtained, ranging from well-known discrete functions (such as Negative Binomial and Poisson) to discretized versions of continuous distribution functions. Table 1 shows the different probability distribution functions assessed in this work. It is worth noting that given that the continuous functions family is larger than the discrete one, most of the bi-parametric functions used here come from discretizing well-known continuous probability distributions [12].
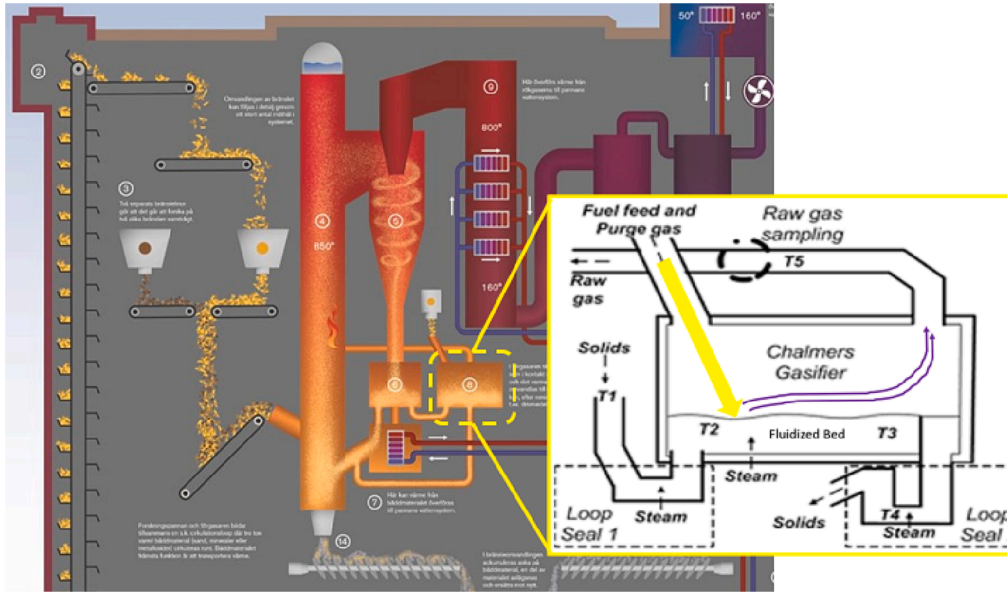
Fig. 3. Schema of the Chalmers DFB Gasifier used in this work (modified from [15]).

Bi-parametric functions are highly adaptable and widely studied functions that describe physical phenomena that occur in many fields. They are sufficiently robust to describe strong variations in a dataset with a high number of outliers. As an example, the highlighted functions in Table 1 (marked with *) are known as heavy-tailed functions, i.e., the tail decays slower than the ones with exponential decay (Weibull is heavy-tailed for $0 \leq b \leq 1$). This characteristic confers upon the functions the potential to be applied to extreme scenarios in which the dataset presents numerous outliers. They are used to describe systems

2.4. Bed's oxygen Transport

To quantify the Bed Oxygen Transport based on the product composition, both the Hydrogen and Oxygen balances must be investigated. When considering the Hydrogen case, fulfilling the elemental balance in Equation (5) implies defining the amount of water that participated in the conversion ($\Delta n_H^{H_2O} = n_H^{H_2O,in} - n_H^{H_2O,out}$).

$$\Delta n_H^{H_2O} = \left(n_{C,tot}^{pf} \sum_{k=1}^{\infty} X_{C,k}^{pf} \gamma_k^{pf} + n_{C,tot}^{of} \sum_{k=1}^{\infty} X_{C,k}^{of} \gamma_{k,eff}^{of} + n_{H,total}^{arom} + n_H^{H_2,out} \right) - \left(n_H^{fuel} + n_H^{H_2,in} \right) \tag{10}$$

that encompass extreme events, such as maximum one-day rainfall levels, river discharges, and survival times associated with medical treatments [13]. It is interesting to notice that although they may appear to be defined different mathematically, some of them can show a similar behavior when evaluated over a large domain. For instance, a quick look at the Fréchet function reveals that it behaves as a power-type distribution, since the expression $1 - e^{-x^\beta}$ is asymptotically equivalent to $k^{-\alpha}$, which means that it will not decay as rapidly as an exponential function but will behave similarly to the Burr function in the infinite.

Overall, irrespective of the type of function, the idea is to take the measured data as anchoring points, the experimental uncertainties as constraints and Equations (4) and (5), to create a new system of equations to find the shape parameters $\{\alpha_i\}$ of the particular function. If a finite and real set of parameters $\{\alpha_i\}$ is found, the respective function will be by consequence a solution to the PSM equation system. Given the nature of most of the distribution functions, non-linear solvers or a Monte Carlo method can be used to perform the task of finding the set of parameters that satisfies the conditions imposed by the system of equations. Once the shape parameters are identified, the function can be plotted on top of a column bar graph depicting the species in *mol/kgf* versus the *k*-groups.

Thus, knowing that water has a H:O ratio of 2:1, Equation (5) can be rearranged in terms of $\Delta n_H^{H_2O}$ and be reinserted into the oxygen balance (Equation (3)), to give Equation (11), according with the next derivation:

$$n_O^{CO} + n_O^{CO_2} + n_O^{HC,out} - \left(n_O^{H_2O,in} - n_O^{H_2O,out} \right) = n_O^{fuel} + n_O^{O_2,in} - n_O^{O_2,out}$$

$$\Rightarrow n_O^{CO} + n_O^{CO_2} + n_O^{HC,out} - \frac{1}{2} \left(n_H^{H_2O,in} - n_H^{H_2O,out} \right) - n_O^{fuel} = n_O^{O_2,in} - n_O^{O_2,out} = \Delta n_O^{ext}$$

$$\Rightarrow \Delta n_O^{ext} = n_O^{CO} + n_O^{CO_2} + n_O^{HC,out} - \frac{1}{2} \Delta n_O^{H_2O} - n_O^{fuel}$$

$$\tag{11}$$

Here, Δn_O^{ext} refers to the reacted oxygen that enters the process from an external source, i.e., oxygen that does not originate from the feedstock itself or the fluidization steam. If positive, it means that external oxygen was consumed during the reaction. If negative, it means that oxygen was removed from the reaction environment by an external agent. For our studied case, there were two identified external oxygen sources: unexpected air leakage into the reactor, and the circulating bed material. The former can be estimated by assuming that all the nitrogen detected in the micro-GC arises from air and by applying the $O_2 : N_2$ ratio of air. This can be done straight away when no other source of nitrogen is present (as for instance in the fuel). Nonetheless, this value tends to be relatively low due to the precautions taken during setup
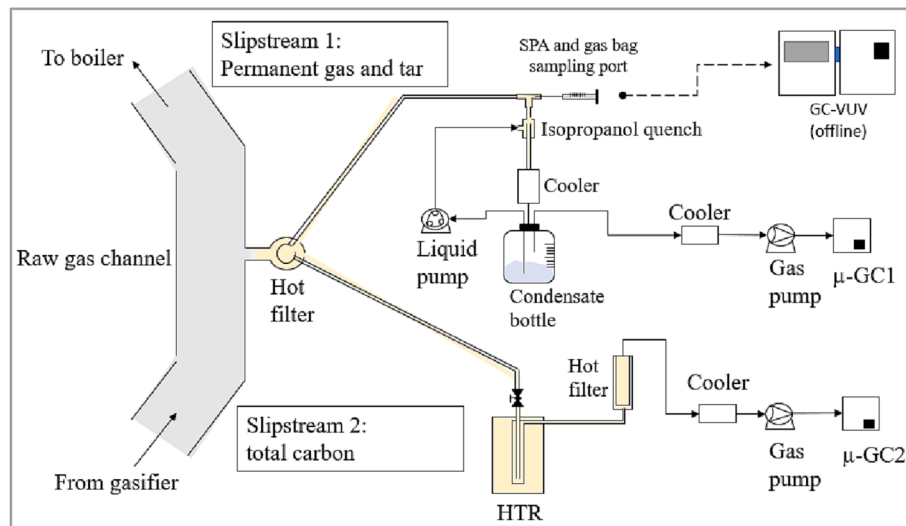
Fig. 4. Gas Sampling Setup connected to the Gasifier's outlet (Modified from [11]).

construction and periodic maintenance to avoid air leaks.

Under usual DFB conditions, Equation (11) is an expression that links the hydrogen balance with the oxygen transported by the bed during the fuel conversion. From the perspective of the model, the parametric functions assigned to the paraffin and olefin species in the hydrogen case (Equation (8)) will contain all the information on the species distribution, so they may be used as a way to estimate the BOT in the pyrolysis system.

An alternative experimental method to quantify the oxygen transport is here applied for the purpose of validating the estimates given by the PSM model. The experimental method is based on a High-Temperature Reactor (HTR) [14] (later described in Section 3), where the gas product reacts further with the steam to generate only syngas. The calculation of the BOT based on the measurements from the HTR is also done by Equation (10) but in a greatly simplified form. In this case, by reforming each and every one of the hydrocarbon species the products out of the reactor will be CO, CO_2 and H_2. Thus, the first parenthesis in Equation (10) collapses into only the Hydrogen measured at the outlet ($n_H^{H_2,out}$ term), as follows:

$$\Rightarrow \Delta n_O^{O_{ext}} = n_O^{CO} + n_O^{CO_2} + n_O^{HC,out} - \frac{1}{2}\left(n_H^{H_2,out} - \left(n_H^{fuel} + n_H^{H_2,in}\right)\right) - n_O^{fuel} \quad (12)$$

The result obtained from Equation (12) must be the same as that estimated by Equation (11), since the measurements came from the same sampled gas batch. Table A5 in the Appendix shows the results obtained from the HTR setup.

2.5. Hydrogen to carbon ratio constraint

An additional constraint is set for the Hydrogen functions and is related to the term $\gamma_{k,eff}^{of}$ presented in Equation (6). This is defined as the effective H/C ratio of the olefin species in each k-group. For each k, this quantity varies between 2 and the lowest possible H/C ratio given the chain length and the carbon valency, i.e., when $g = 2\lfloor k/2 \rfloor - 1$. The olefin's Hydrogen function will be constrained in a region formed by the function $f_H^{high} = 2n_{C,k}^{of}$ (only mono-enes) and the fully unsaturated scenario, $f_H^{low} = \frac{1}{k}((2k+2) - 4\lfloor k/2 \rfloor)n_{C,k}^{of}$, when every possible hydrogen has been extracted from the chain of the group k. An intermediate case can also be defined, and this is the fully conjugated one, $f_H^{mid} = \frac{1}{k}((2k+2) - 2\lfloor k/2 \rfloor)n_{C,k}^{of}$, where the chain only contains intercalated double bonds along its length. Any of the olefin's Hydrogen functions must be within this range to fulfil the chemical characteristics of the molecular system.

3. Experimental setup

The data used in the present work were obtained from experiments carried out in the 2–4-MW DFB gasifier of the Chalmers Power Central facility. Here, the fluidized bed gasifier is coupled with a 12-MW Circulating Fluidized Bed combustor that fed with biomass wood chips (see Fig. 3).

The gasifier is fluidized with steam, using silica sand as bed material, and it is operated in high-temperature pyrolysis mode, i.e., 750°–850 °C. To create the bulk of data to test the model, different experiments were performed using polyethylene (C: 84%w, H: 15%w) as the feedstock, and under different conditions of temperature and steam-fuel ratio. The silica sand, biomass and ash compositions as well as the operative conditions can be found in Table A1 to Table A4 of the appendix respectively.

A sampling stream was taken from the product gas at the reactor's exit, and it was split in two. One part went to an isopropanol quench loop that washes out the aromatics, long hydrocarbon chains and water from the gases. Thereafter, the gases are cooled further (effectively to ∼ 0 °C), so as to guarantee that there is no downstream condensation of species (only survived by C4 species and below), and then pumped into the Varian CP4900 micro-GC (GC1) with TCD detector, where the H_2, C1, C2 and C3 species were quantified online. Before going into the isopropanol quench loop, there is a septa port through which aromatic samples are acquired using the solid-phase adsorption (SPA) method. In brief, 100-mL of raw gases are sucked through an adsorbent column, which consists of a layer of activated carbon followed by an amine absorbent layer (Supelclean ENVI-Carb/NH2 SPE columns). The content of the vial is subsequently analyzed in a Bruker GC430 gas chromatograph coupled with a flame ionization detector (FID). In the same point, a gas sample was taken for the characterization of C4+ species in an offline GC-VUV chromatograph. The second slipstream was sent for full steam reforming at 1700 °C in the High Temperature Reactor (HTR), with subsequent online characterization of the gases in another similar micro-GC (GC2). A detailed description of the experimental and sampling setup can be found elsewhere [11], and a schematic of the sampling setup is presented in Fig. 4.

The purpose of the HTR reactor in this work was double fold. Firstly, it was used for measuring the total carbon and indirectly estimate the yield of char. And secondly, it served as the experimental tool to measure the Bed's Oxygen Transport (BOT) and thereby validate the model estimations. Regarding the BOT in the system, the silica sand contains small amounts of Fe_2O_3 and the biomass used in the combustor also contained traces of sulphur, iron and other transition metals that tend to
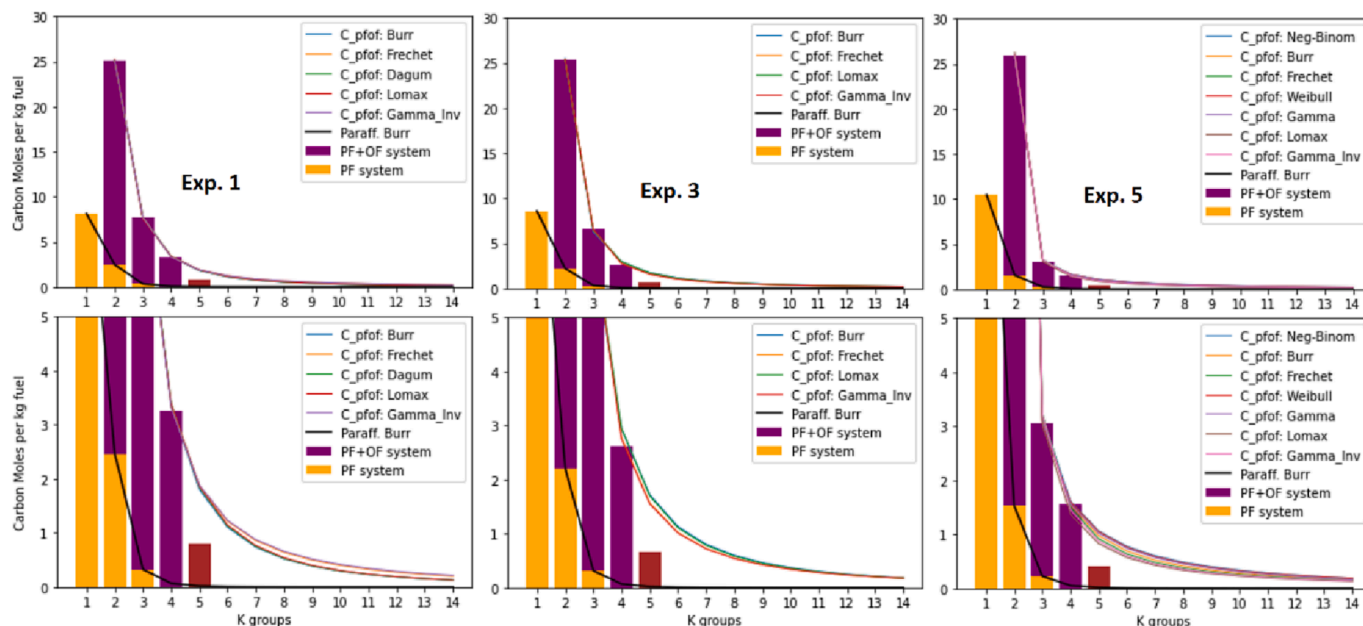
Fig. 5. Results of some of the parametric functions tested upon the species' carbon distribution, expressed in $molC/kg_{fuel}$ vs. k-group, obtained at different severity cases (Exp 1, 3 and 5 from left to right). The results are considered for the paraffins and olefins cases. Bottom row: Zoomed-in plots. (Red column: incomplete group species measured). (For interpretation of the references to colour in this figure legend, the reader is referred to the web version of this article.)

Table 2
Results of the total area, tail area (sum of C5 +), and the parameters associated with the functions tested. (Nan = No results; *= Heavy-tailed functions).

	Exp 1				Exp 3				Exp. 5			
Function	Area	Area Tail	α1	α2	Area	Area Tail	α1	α2	Area	Area Tail	α1	α2
Neg-Binom	nan	nan	nan	nan	nan	nan	nan	nan	35.079	11.480	0.943	0.128
Con-Max	nan	nan	nan	nan	nan	nan	nan	nan	nan	nan	nan	nan
Burr *	40.048	10.742	1.204	1.117	40.323	13.025	1.243	0.867	36.204	12.574	1.620	0.465
Frechet *	42.774	13.965	0.854	0.589	40.254	12.788	0.811	0.481	36.281	12.080	0.498	0.158
Dagum *	40.077	10.789	0.442	1.399	nan	nan	nan	nan	nan	nan	nan	nan
Gompertz	nan	nan	nan	nan	nan	nan	nan	nan	nan	nan	nan	nan
Weibull *	nan	nan	nan	nan	nan	nan	nan	nan	36.164	13.042	0.686	0.315
Gamma	nan	nan	nan	nan	nan	nan	nan	nan	34.500	10.594	0.066	0.126
Lomax *	40.134	10.865	2.538	1.380	40.335	12.994	1.949	0.691	35.713	11.120	1.444	0.076
Gamma_Inv *	43.458	14.631	0.760	0.429	40.438	12.940	0.744	0.342	36.122	11.622	0.439	0.061

accumulate in the bed, along with 22% of calcium in the ashes [16,17]. Thus, it was expected that some oxygen be transported by the bed material in this reactor's system. The detailed description of the HTR is presented elsewhere [14]. The results obtained from GC1 and GC2 are reported respectively in Table A4 and Table A5 in Section 7.3 of the Appendix.

Furthermore, to test the capabilities of the model in assessing the quality of experimental data, an out-of-range calibration curve was used to induce a systematic error in the measured concentration of certain measured species. This will be further discussed in Section 4.3. The maximum concentrations used on this calibration as well as the species data obtained with the out-of-range calibration are shown in Table A7 and Table A8, for GC1 and GC2 respectively. As shown in Table A7, some of the species surpassed by 4 or 5 times the maximum value of the %vol calibration. A similar situation is presented also with the GC2 measurements in Table A8, where the %vol for H_2 was somewhat higher than the maximum calibration point. Note that this set of data also gave a more skewed carbon distribution, which has been applied to the model for testing its robustness as described in Section 4.1.

4. Model results and discussion

4.1. Assessment of function's suitability

As explained in Section 2.2, to apply the concept underlying the PSM, a function with the minimum number of shape parameters (α) must be found that fulfills the data topological conditions and the carbon balance. After testing the functions presented in Table 1, it was found that the high variability of adjacent species in the measurements prevented a good fit for the mono-parametric functions evaluated (Geometric, Poisson and Flory-Schultz). Therefore, an additional parameter was required to facilitate better control of the decaying behavior of the distribution in the tail and in lower *k*-groups. Taking advantage of the number of observables obtained for each molecular system, ($C1, C2, C3$) for paraffins and ($C2, C3, C4$) for olefins, the bi-parametric functions can be related to the ratios among adjacent *k*-groups, to derive a closed system of equations. (C5 is not considered a reliable observable to fit the function, since only two out of approximately ten possible olefin species could be measured with the analytic instruments applied).

Although most of the bi-parametric functions in Table 1 adapted very well to the paraffin system measurements, very few complied with the characteristic skewness imposed by the large ratios found in adjacent *k*-groups for the olefins case. In general, the heavy-tailed functions of Table 1 were those that presented the highest degree of flexibility to
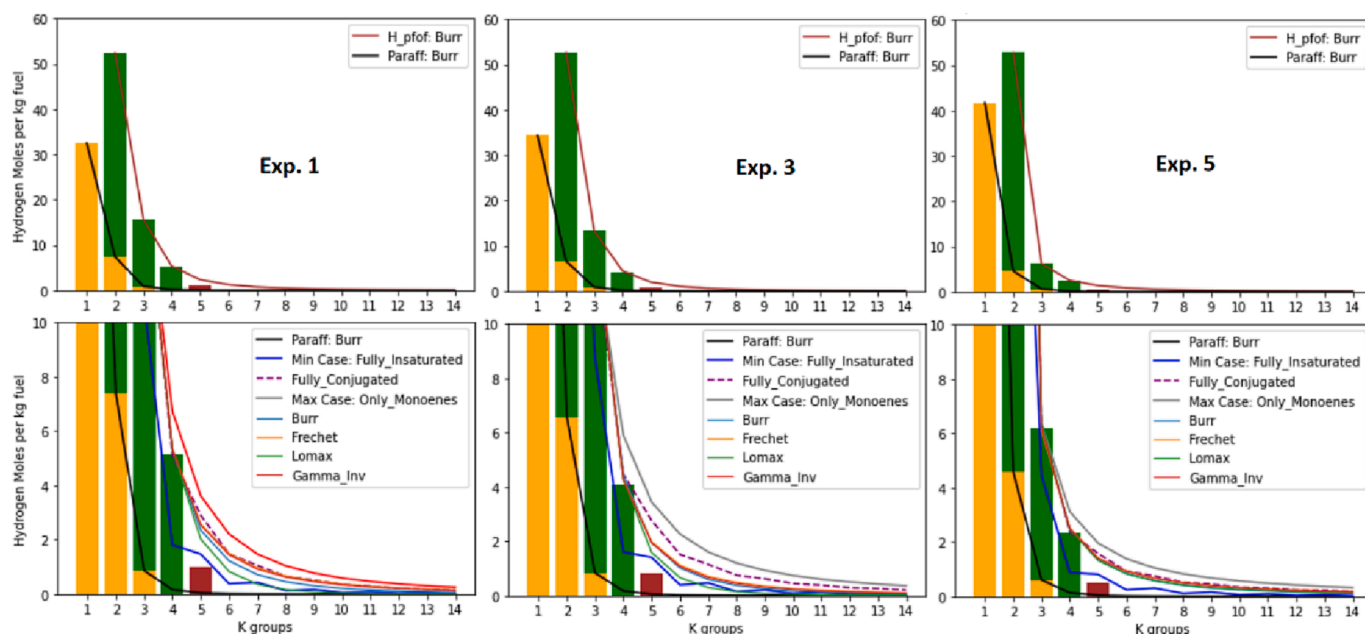
Fig. 6. Results of the discriminated parametric functions applied to the Hydrogen distribution of the species, expressed in molH/kg$_{fuel}$ vs. k-group, for Experiments 1, 3 and 5. Upper row, Burr function results. Bottom row, zoom in and evaluation of the functions according with the gamma effective. (Red column: incomplete group species measured). (For interpretation of the references to colour in this figure legend, the reader is referred to the web version of this article.)

Table 3
Bed's oxygen transport calculated from the HTR and estimated from the model (PSM).

BOT HTR	BOT PSM	%dif
8.27	8.91	7.74
10.8	9.52	11.85
10.21	9.51	6.86
8.92	8.87	0.56
8.14	7.18	11.79

Table 4
BOT results obtained from HTR and PSM in the miss calibrated data case.

BOT HTR	BOT PSM
15.62	5.49
16.48	6.56
15.72	6.79
14.23	5.68
17.18	8.24

satisfy the system conditions. Fig. 5 shows the results obtained for the carbon moles per kilogram of fuel vs. the *k*-group when the functions were applied to Experiments 1, 3 and 5 (from left to right) for the data shown in Table A4. Although the study was performed for all five experiments, for graphical purposes, only these three cases are shown due to their relevance in terms of the ranges of severity achieved in this work (severity was measured as the ratio of the ethylene to the propylene carbon moles). The bars in the upper row of Fig. 2 show the experimental results for paraffin (orange) and aggregated paraffins and olefins (purple), and the different functions applied to describe the systems. The "*pfof*" function refers to the one formed by summing the paraffin and olefin functions for each *k*. The bottom row of Fig. 2 is a zoomed-in version of the respective figures in the upper row. The different paraffin functions tested showed no appreciable difference in terms of the area prediction (total moles of carbon). However, the Burr function was the only one capable of handling large ratios between adjacent k-

groups; so, this is the only function that will be shown here for the paraffin system. C5 is shown in a red column due to the lack of species data, which is attributed to equipment constraints.

As can be seen in Fig. 5, the bi-parametric functions overall describe well the data behaviors in the experiments, within the experimental uncertainty intervals for each carbon group. The heavy-tailed functions Burr, Fréchet, Lomax and Inverse Gamma (Gamma_Inv) were the only ones flexible enough to fit the data at all severity levels. It is a characteristic of these kind of functions that their tails stretch out over longer carbon groups with a lower decaying rate, which has an enlargement effect on their total enclosed areas, i.e., on the total carbon moles predicted, as can be seen in Table 2. This is an important characteristic specially in low severity cases where long chain species are expected to be present after the cracking process. At high severities, the long chains start to disappear to produce shorter hydrocarbon species causing the observed increase in the data skewness. Also, topologies with a fast-decaying behavior and relatively low estimated areas are able to fit in such a skewness, e.g. Negative Binomial and Gamma, as presented in Table 2 results. Nonetheless, even in this case, still the set of heavy-tailed functions mentioned previously were flexible enough to keep up with the high-level skewness of the experimental data without causing a significant difference in the total area. This exemplifies the robust nature of this family of functions when working in cases with large and low ratios between the carbon groups.

Table 2 shows the results for the area predicted, tail area (sum of the C5 + species prediction), and the parameters for each evaluated olefins function in the selected experimental cases (Experiments 1, 3 and 5).

As mentioned before, from Table 2 it is possible to see that the heavy-tailed function distributions (asterisk marked), in general predicted a greater area, i.e., more total moles for the olefins system than for the non-heavy-tailed ones. Overall, with the set of functions that could fit all the experimental cases, a prediction uncertainty range could be established for the C5 + species between the functions with the minimum and maximum areas. This range can be narrowed down by discarding functions that do not fit into the hydrogen constraints for the molecular system (this will be analyzed later). A further reduction can be obtained either by acquiring data for larger *k*-group species or by exploring in greater detail the statistical characteristics of the chemical system.

Table 5
Percentage difference of the out-ranged species due to the miss calibration with respect to the original calibration.

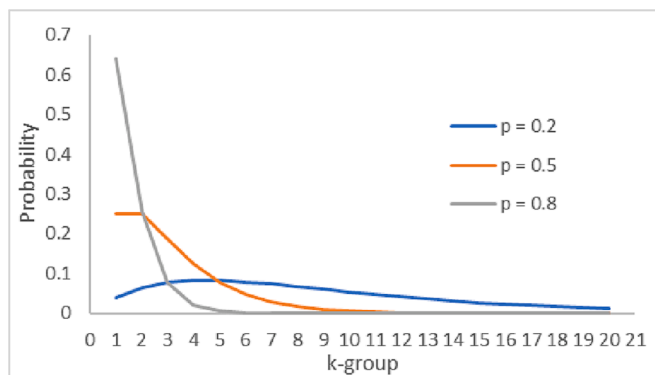| CH4	C2H4	C2H6	C3H6	C3H8	Average
−8.68	−11.94	−7.57	−21.15	−4.52	−10.77
−8.62	−11.93	−7.07	−21.14	7.82	−8.19
−8.94	−11.94	−6.76	−21.15	−4.05	−10.57
−9.13	−11.93	−6.64	−21.10	0.00	−9.76
−9.34	−11.94	−2.21	−20.80	−10.00	−10.86
				Global Avg. (%)	**−10.03**

Fig. A1. Simplified view of the breakdown process. (Flory-Schultz distribution).

However, probing in-depth into the kinetics and physical nature of the pyrolysis phenomena to discover which function could be most suitable from a mathematical perspective will be a topic for future research.

Regarding the Hydrogen distribution case, Fig. 6 shows the same experimental cases as in Fig. 5. For graphical purposes and adaptableness reasons that will be presented later, only the Burr function is shown in the upper row plots in Fig. 6. Nevertheless, in the plots in the bottom row, which present zoomed-in versions for the evaluated experimental cases, all the tested functions are shown.

The graphs in the bottom row of Fig. 6 show the allowable hydrogen per *k*-group. The grey, blue and purple-dashed curves correspond respectively to the three theoretical scenarios of only mono-enes, the fully unsaturated and fully conjugated case of the olefin's gamma effective function ($\gamma_{k,eff}^{of}$) introduced at the end of Section 2.5. As shown in the bottom row of graphs, for C7 + species, not all functions stayed within the allowed range of hydrogen, with the exception of Burr, Fréchet and Inverse Gamma, which were within range for all the *k*-groups and all the experimental cases. This means that these three functions have such a shape that its predicted hydrogen quantities for C5 + species satisfy the chemical characteristics of the olefin system, which provides greater confidence regarding their estimations.

As a robustness test, the functions were tried out in a more drastic skewed scenario using the data coming from the out-of-range calibration test mentioned at the end of Section 3. In Fig. A2 and Fig. A3 of the appendix, the results for the carbon and hydrogen data are shown respectively. From the test, Burr was the only function that could keep up with the even higher data skewness while still fulfilling the systems constraints. Hence, given its robustness for all tested cases, Burr was the selected function for the analysis done in the next sections, and it is the function recommended in this work for the PSM application at the evaluated process conditions.

4.2. Validation of the model's outcomes

Once the complete hydrogen series of paraffins and olefins are defined by suitable functions, i.e., enclosed within the PSM framework, Equation (11) can be used to calculate the Bed's Oxygen Transport (BOT) in the reactor. On the other hand, the experimental setup includes an HTR reactor capable of reforming all the hydrocarbons coming from the process. As pointed out in Section 2.4, the results derived from this setup can be used as validation because it is based on the fact that the BOT estimated by PSM must render the same results as as Equation (12), which is based on the HTR setup, since they originate from the same sampled chemical system (see Fig. 4). In Table 2 the reader can find the results of the BOT calculated from the HTR results and the PSM estimation respectively. Also, in Table A6 in the appendix, the reader is

Fig. A2. Results of some of the parametric functions tested upon the species' carbon distribution, expressed in molC/kg_fuel vs. k-group, obtained from the study case of miss-calibrated species for Experiments 1, 3 and 5 (from left to right). The results are considered for the paraffins and olefins cases. Bottom row: Zoomed-in plots. (Red column: incomplete group species measured). (For interpretation of the references to colour in this figure legend, the reader is referred to the web version of this article.)
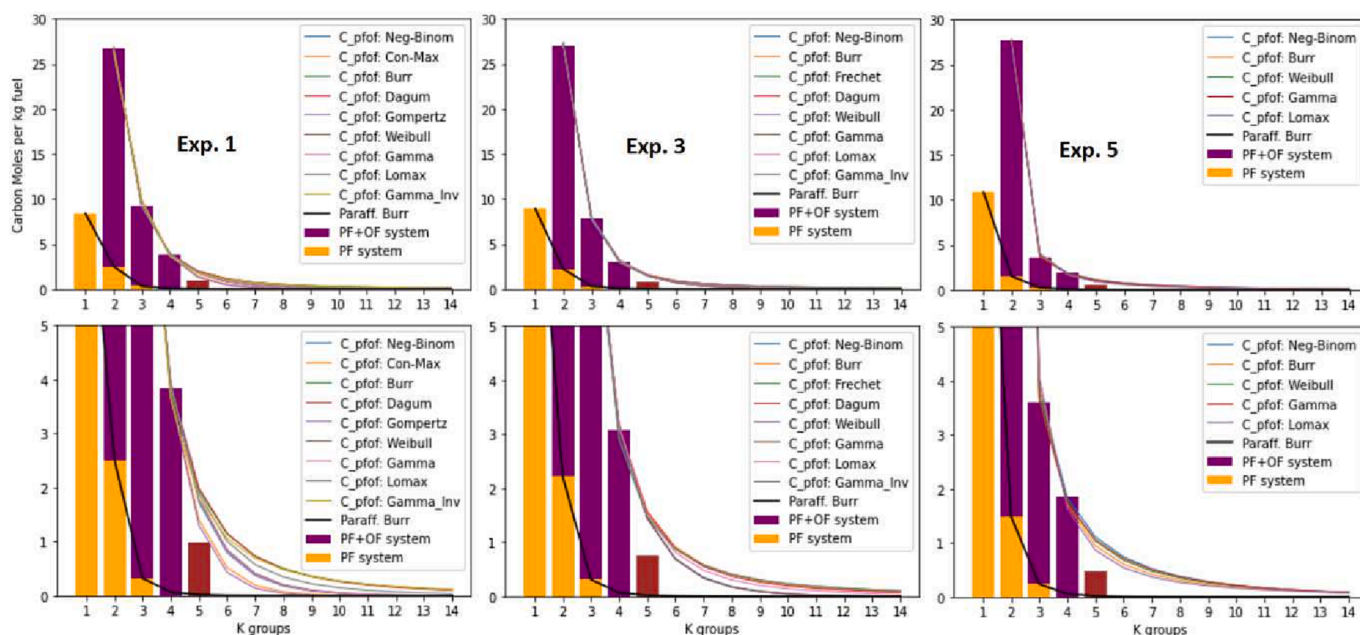
Fig. A3. Results of some of the parametric functions tested upon the species' Hydrogen distribution, expressed in molC/kg_fuel vs. k-group, obtained from the study case of miss-calibrated species for Experiments 1, 3 and 5 (from left to right). The results are considered for the paraffins and olefins cases. Bottom row: Zoomed-in plots. (Red column: incomplete group species measured). (For interpretation of the references to colour in this figure legend, the reader is referred to the web version of this article.)
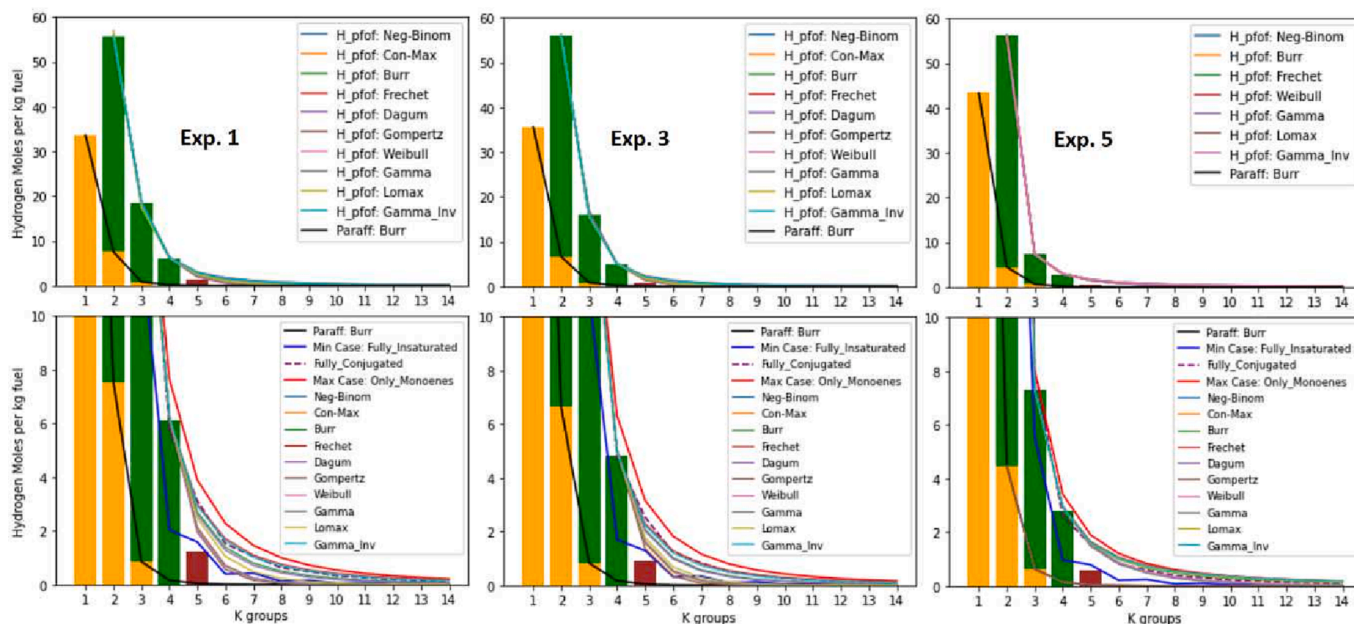
invited to check that the transported oxygen calculated by HTR per kg of bed material circulation is in line with the value measured in other experiments using silica sand as the bed material in the Chalmers boiler, i. e., $0.1\%w/w_{BM}$ (see [3]).

As it is possible to observe in Table 3 all the model BOT values calculated using PSM present an error of $< 12\%$ with respect to the values given by the HTR. This is acceptable, considering other random errors that can be involved in the unavoidable variations of a large-scale process or even due to the intrinsic numerical uncertainty of the model when predicting the carbon and the hydrogen tail.

4.3. Data quality assessment

In order to evaluate the capabilities of the model for data quality assessment, the data was then altered by taking calibration curves which contain certain species out of calibration range. The results and functions for the carbon and hydrogen of the new data are shown in Fig. A2 and Fig. A3 of the appendix respectively. As mentioned previously, this case was highly skewed, and Burr was the only function that proved robust enough to keep with such extreme case. When applying Equation (12) to calculate the BOT by the HTR results and Equation (11) to calculate it by the PSM, the results with the new altered data are shown in Table 4.

As it is possible to observe in Table 4, now there is a significant mismatch between the results obtained with the two approaches indicating the presence of an inconsistency. No matter which function was used or which experimental case was evaluated, the BOT value calculated using Equation (12) based on the HTR measurements was 2–3-fold higher than that estimated by PSM from Equation (11). When checking the predictions made by the method for the olefins, it became apparent that the measured species occupy between 80 and 90% of the functions area (see Table 2). Given the topological constraints of the functions tail,

Table A1
Typical silica sand composition used as the bed material in the Chalmers DFB gasifier (See [3]).

Comp.	%wt
SiO_2	88–92
Al_2O_3	4.5–6.6
Fe_2O_3	0.4–0.7
K_2O	0.9–2.7
Na_2O	1.0–1.4

Table A2
Typical averaged elemental compositions of the biomass used as a feedstock in the Chalmers gasifier (See [15,21]). %w$_{db}$: weight percentage dried basis.

Parameter	Wood Chips	Method
C [%w$_{db}$]	49–50	SS_EN_ISO 16,948
H [%w$_{db}$]	6–6.2	SS_EN_ISO 16,949
O [%w$_{db}$]	43	By difference
N [%w$_{db}$]	0.11–0.13	SS_EN_ISO 16,948
S [%w$_{db}$]	<0.02	SS_EN_ISO 16,994
Cl [%w$_{db}$]	<0.01	SS_EN_ISO 16,994
LHV [MJ/kg$_{db}$]	18.7–18.3	ISO-1928
Ash [%w$_{db}$]	0.5–0.7	SS_EN_ISO 18,122
Moisture [%w]	36–47	Difference wet - dry

Table A3
Elemental compositions of the ashes in the Biomass used as a feedstock in the Chalmers gasifier. The column "Ash Rel." refers to the percentage relative to the biomass ash fraction (See [15,21]). %w$_{db}$: weight percentage dried basis.

Element	%w$_{db}$	Ash Rel. (%)
Al	0.002	0.4
Si	0.008	1.4
Fe	0.002	0.4
Ti	<0.001	<0.3
Mn	0.006	1.1
Mg	0.022	3.8
Ca	0.130	22.3
Ba	0.001	0.2
Na	0.005	0.9
K	0.082	14.1
P	0.010	1.7

Table A4

Measurements obtained from the gas species obtained from the steam pyrolysis of Polyethylene. SG, Steam to gasifier flow; SE, steam to extruder flow; TPD, temperature particle distributor (T1 in Fig. 3); TG1, temperature of the gasifier (T2); TRG, temperature of the raw gas (T5); BM, bed material flow; He, helium gas flow. The experiments are sorted according to process severity, defined here as the ratio of the ethylene to the propylene carbon moles.

Operative Conditions					
Variable	EXP 1	EXP 2	EXP 3	EXP 4	EXP 5
Feedstock	Polyethylene	Polyethylene	Polyethylene	Polyethylene	Polyethylene
Feed (kg/h)	90	90	90	90	90
SG (kg/h)	150	150	150	150	150
SE (kg/h)	80	80	80	80	80
TPD (°C)	833	830	822	807	870
TG1 (°C)	781	787	788	793	843
TRG (°C)	710	717	723	717	762
BM (ton/h)	16.9	15.7	21.2	22.7	28.1
He (L/min)	35	35	35	35	35
Products (kg/kgf)					
H2	0.012	0.013	0.014	0.013	0.022
CH4	0.130	0.128	0.137	0.141	0.167
CO	0.017	0.017	0.018	0.022	0.027
CO2	0.076	0.107	0.085	0.073	0.128
C2H4	0.313	0.312	0.320	0.311	0.333
C2H2	0.004	0.003	0.004	0.004	0.008
C2H6	0.037	0.034	0.033	0.032	0.023
C3H6	0.103	0.102	0.087	0.083	0.038
C3H8	0.005	0.010	0.005	0.006	0.003
C4H6	0.037	0.037	0.030	0.029	0.020
C4H8	0.007	0.007	0.005	0.006	0.001
C4H10	0.000	0.000	0.000	0.000	0.000
C5HX	0.054	0.040	0.045	0.044	0.027
H2S	0.010	0.011	0.003	0.003	0.003
Aromatics (kg/kgf)					
Benzene	0.092	0.090	0.093	0.108	0.117
Toluene	0.029	0.025	0.025	0.027	0.022
Xylenes	0.002	0.002	0.002	0.003	0.001
Styrene	0.014	0.014	0.014	0.016	0.018
Naphthalene	0.016	0.016	0.017	0.019	0.030
Anthracene	0.001	0.001	0.001	0.001	0.001
Other arom.	0.024	0.023	0.024	0.026	0.033
Soot	0.399	0.081	1.115	2.179	2.424
Total	1.380	1.075	2.078	3.146	3.447

Table A5

Measurements obtained from the HTR setup.

Operative Conditions					
Variable	EXP 1	EXP 2	EXP 3	EXP 4	EXP 5
HTR temp. (°C)	1700	1700	1700	1700	1700
Products (kg/kgf)					
H2	0.298	0.296	0.293	0.282	0.291
CH4	0.008	0.000	0.000	0.013	0.001
CO	1.551	1.566	1.509	1.436	1.426
CO2	0.586	0.611	0.611	0.587	0.624
C2H4	0.000	0.000	0.000	0.003	0.000
C2H2	0.000	0.000	0.000	0.000	0.000
C2H6	0.000	0.000	0.000	0.000	0.000
C3H6	0.000	0.000	0.000	0.000	0.000
C3H8	0.000	0.000	0.000	0.000	0.000

Table A6

Beds Oxygen Transport values based on the HTR results for each experiment. BM, bed material circulation flow.

Exp.	mol O/kg$_{fuel}$	mol O/kg$_{BM}$	kg$_O$/kg$_{BM}$ (%)
1	8.27	0.03	0.04
2	10.80	0.05	0.07
3	10.21	0.06	0.09
4	8.92	0.05	0.08
5	8.14	0.03	0.05

there was insufficient area remaining to predict a probabilistic meaningful share of the unknown species (C5 +) for each *k*-group. This indicates the systematic error that is affecting the measurements, resulting in inflation of their quantities, which translates into a lower BOT value predicted by Equation (11). In fact, the overestimation in terms of the moles of the measured species must be on average for all the experiments around 15%, to ensure that the PSM estimation matches the HTR measurement.

In conditions where no information of the discrepancy's origin is known before hand, such an error can be explored either in the calibration of the analytical instrument, environmental changes or inadequate methods of observation. For instance, in this case, it is possible to observe in Table A7 of the appendix that the sum of the volume concentrations of the species detected by the micro-GC1 (see Fig. 4) was > 100%, which is a clear support to place the inaccuracies in the analytical instrument calibration. Indeed, given the sampling system, the total detected species concentration is expected to be < 100%. The carbon-containing species detected by GC1 were those in the range of C1–C3. However, the setup connected to that chromatograph is cooled effectively to a point where, based on the boiling temperatures, it becomes highly likely that the C4 species will also reach the micro-GC (~0 °C). According with the GC-VUV results, C4 species must account for 2–5 % vol of the final gas; therefore, the total sum of species detected by the micro-GC1 should be around 95–98 %vol.

Table A7
Volume concentrations of the species measured in GC1 (main sampling line). The "Max. Calib." column lists the maximum volume concentrations used to build the GC calibration curves used in this work. The asterisk marked species were outside the maximum calibration point.

| Species | Volumen Concentration (%vol) GC1 | | | | | | |
	Exp. 1	Exp. 2	Exp. 3	Exp. 4	Exp. 5	Exp. 6	Max. Calib.
He	2.964	3.032	3.046	2.997	3.007	2.625	14.973
H2	14.407	15.380	17.040	18.528	16.242	24.628	50.050
O2	0.305	0.253	0.288	0.292	0.338	0.444	0.501
N2	7.997	5.372	5.041	5.507	9.212	5.525	94.273
CH4 *	28.084	24.423	24.206	25.625	26.440	27.360	16.009
CO	2.216	1.655	1.693	1.748	2.111	2.250	39.428
CO2	4.979	5.301	7.363	5.835	5.082	7.588	69.893
C2H4 *	29.125	34.880	34.839	35.237	34.321	32.134	5.003
C2H2	0.454	0.441	0.417	0.508	0.474	0.860	1.001
C2H6 *	3.232	3.657	3.354	3.195	3.133	1.868	0.508
C3H6 *	11.326	8.512	8.497	7.138	6.810	2.746	0.498
C3H8 *	0.524	0.310	0.588	0.296	0.400	0.200	0.501
H2S	0.179	0.728	0.831	0.291	0.232	0.214	0.503
Total	105.791	103.944	107.203	107.197	107.802	108.440	

Table A8
Volume concentrations of the species measured in GC2 (HTR line). The "Max. Calib." column lists the maximum volume concentrations used to build the GC calibration curves used in this work. The asterisk marked species were outside the maximum calibration point.

| Specie | Volumen Concentration (%vol) GC2 (HTR) | | | | | | |
	Exp. 1	Exp. 2	Exp. 3	Exp. 4	Exp. 5	Exp. 6	Max. Calib.
He	0.468	0.400	0.487	0.494	0.517	0.494	14.973
H2 *	65.553	53.338	64.751	65.213	66.208	64.696	50.050
O2 *	0.641	4.170	0.800	0.707	0.553	0.837	0.501
N2	2.803	14.260	2.866	2.654	2.942	3.154	94.273
CH4	0.327	0.197	0.000	0.000	0.405	0.000	16.009
CO	24.656	20.198	24.631	24.147	24.227	23.880	39.428
CO2	6.493	5.035	6.351	6.463	6.519	6.683	69.893
C2H4	0.000	0.000	0.000	0.000	0.000	0.000	5.003
C2H6	0.000	0.000	0.000	0.000	0.000	0.000	1.001
C2H2	0.000	0.000	0.000	0.000	0.000	0.000	0.508
C3Hx	0.000	0.000	0.000	0.000	0.000	0.000	0.498
Total	100.941	97.597	99.886	99.679	101.371	99.744	

After calculating the percentage difference for the miss-calibrated species in GC1 (see Table 5), the global averaged discrepancy (10.03%) is of the same order of magnitude as the PSM prediction (15%), which confirms once again the model's error estimation. This outcome reveals the high potential of the PSM approach to identify shortcomings in the quality of the experimental data, where further research could be performed to refine the PSM implementation to achieve an error allocation for each measured k-group.

4.4. Final Remarks

As shown here, the reduction in the degrees of freedom of the measured system, ranging from a whole list of experimentally determined species to just two parameters that shape a specific distribution function, allows the PSM to capture and compress the information in such a way that useful knowledge can be extracted. The important results obtained show that, in terms of data representation, the PSM has great potential to become a versatile tool, not only for use in the prediction of unknown data, but also to improve measurement accuracy and ensure that the measurements make statistical and chemical sense in line with the evaluated system.

In practical applications, the ability of the model to estimate the share of non-measured C5 + carbon species could be valuable for any pyrolysis process, especially for the downstream operation of a refinery connected to such a process. Furthermore, the model's concept of condensing the data into a constrained function with a set of parameters opens the possibility to characterize not only the results of the pyrolysis process but the process itself; and this is where it shows its full potential.

The results of the chemical system created by the process conditions define a particular function profile that corresponds to a unique set of

shape parameters. In general, each set of process conditions defines a hyper-state in the infinite multidimensional space formed by the permutations of the key operative variables, e.g., the feedstock type, bed type, temperature, steam-to-fuel ratio, etc. In the same manner, the shape parameters can form an infinite space, although they may have equal or less-complex dimensionality. In sets theory, if both spaces share the same cardinality (same size), there exists a bijective transformation, albeit non-linear, that connects the operative space with the one formed by the shape parameters. In practical terms, this means that a set of shape parameters can map into a single hyper-state of operative conditions. Therefore, the resulting model's statistical function can be regarded as a signature, or fingerprint, of the process under a specific set of conditions. Each time that the conditions are met, the signature will appear. Consequently, the model can be used as a means to propagate the system's information in two ways, and to obtain useful outcomes from them. In the first way, operational conditions are introduced, and the model will predict the process outputs. This can be considered as forward propagation of the information. In the second way, the process outcomes are given as an input to go backwards into the model and determine the conditions that yielded these results. This corresponds to backward propagation.

5. Conclusions

A Parametric System Model (PSM) was developed to represent the data emerging from a steam pyrolysis process. The main characteristic of the PSM is that it contains generic knowledge of the evaluated chemical system in terms of conservation laws and probabilistic properties. By including elemental (C, H, O) balances and a topology that has statistical meaning, it encloses the system in a way that useful information can be

extracted. Three main outcomes from the model were identified in this work:

1) Based on fitting tests performed with a list of different kinds of known statistical functions, the PSM approach is able to compress the species' carbon and hydrogen data, from a long table of measurement data, into bi-parametric statistical functions. The heavy-tailed distributions as Burr, Fréchet and Inverse Gamma, were the functions that best represented the provided data within the model's constraints. Among them, the Burr function exhibited the highest levels of flexibility against all the different grades of data skewness caused by the process severity, while still retaining the fundamental chemical characteristics of the system (as the total allowed hydrogen in the olefin species).

2) The provided functions' robustness and good fit to the measured data, also shown the PSM's possibility to render estimations of unmeasured carbon group species in the gas product due to characterization equipment constraints. In that way, the model allowed to fully describe the carbon and hydrogen balance of the aliphatic systems (paraffins and olefins) to estimate important process quantities as the Beds Oxygen Transport (BOT) with good approximation respect to the experimental determination in an HTR setup.

3) After inducing some error in the provided data, the capabilities of the model to identify shortcomings in the quality of the experimental data were shown. The PSM outcomes in the BOT calculation allowed to pinpoint and estimate with good approximation the existence of the systematic error that was affecting the species measurements. This revealed the high potential of the PSM approach for data quality assessment and brings forth the possibility to refine the PSM implementation for allocation of the error at each measured k-group.

In general, this work shows the potential of the PSM for application not only as a predictive method but also as a way to improve the quality of the measurements. In that context, the ability of the model to profile the shares of the whole carbon group set in the gas product suggests valuable applications in the control and design of biorefineries connected to a pyrolysis process. Along with that, this study establishes the grounds for further development of the model towards usage for pyrolyzer downstream predictions, as well for evaluations of key upstream conditions.

CRediT authorship contribution statement

Renesteban Forero-Franco: Conceptualization, Methodology, Investigation, Data curation, Formal analysis, Software, Resources, Writing – original draft, Visualization. **Teresa Berdugo-Vilches:** Writing – review & editing, Conceptualization, Visualization. **Chahat Mandviwala:** Resources, Investigation, Writing – review & editing. **Martin Seemann:** Supervision, Project administration, Writing – review & editing. **Henrik Thunman:** Supervision, Conceptualization, Writing – review & editing, Project administration, Funding acquisition.

Declaration of Competing Interest

The authors declare that they have no known competing financial interests or personal relationships that could have appeared to influence the work reported in this paper.

Data availability

Data will be made available on request.

Acknowledgments

Appendix

Remarks About the Functions Topology

As presented in Section 2.3, the function used in the model must satisfy the following conditions: 1) it must present a decaying behavior with the possibility of becoming a monomodal and positively skewed function; 2) it must be sufficiently flexible to allow relatively large changes in the concentrations of species while still fitting with the measured data; 3) it needs to be defined with as few parameters as possible; and 4) the function's form and predicted area must be such that the conservation laws are satisfied.

The first condition is based on the characteristic decaying form of the measured paraffin and olefin data when the species are grouped together according to carbon group (see Section 4 and reference [18] for typical results for the polyolefin pyrolysis process). This distributed behavior is a result of the free radical-mediated breakdown process suffered by the feedstock hydrocarbon chains as soon they enter the hot reactor medium. The pyrolytic reaction progresses as the resulting molecules try to find more-stable structures and lengths. As a rule of thumb, the shorter the chain, the more stable it becomes.

This degradation process can be regarded as stochastic in nature, albeit governed by particular reactions and probabilistic behaviors [19]. In its simplest form as a concept, consider the chemical system as being comprised of two kinds of elements: broken and unbroken bonds. If N_0 is the number of initial bonds, the probability p of finding a bond in the chemical system is defined as $q = N_b/N_0$, with N_b being the number of remaining bonds at time t. Then, the probability of finding a broken bond is $p = 1 - q$ (this also could be seen as the probability of breaking a bond at time t). Let us make blinded pick-ups from that system. The probability of finding n consecutive unbroken bonds in n number of pickups is defined as q^n. A chain molecule of k carbons consists in a set of $k - 1$ unbroken bonds and 2 broken bonds at its extremities. Therefore, the probability of finding such a set of elements in the system will be $p^2 q^{k-1}$. Now, from the carbon's perspective, the probability of finding a particular carbon in such a set will be $P_k = kp^2 q^{k-1} = kp^2(1-p)^{k-1}$. This distribution is commonly known as Flory-Schultz, and it is a special case of the Negative Binomial Distribution for $k - 1$ successes and exactly 2 failures (see Fig. A1).

This simple conceptualization is used merely to highlight the probabilistic nature of the process involved. However, it is useful to understand how the shorter C1, C2 and C3 chains start to show up and become more abundant while the probability of finding longer chains will decrease in an exponential way as the reaction time progresses. The behavior will become more pronounced as the severity of the process increases, which in the given example is equivalent to an increase of the probability p. Though the real case may be more complex, this simplified view offers a reasonable picture of the stochastic process that leads to the results obtained. As an application example of this concept, Zhao et. al. [20] applied this distribution as a first order approximation on top of the carbon number distribution of the products of Polyethylene pyrolysis.

The second and third conditions are grounded in the requirement that the model should be sufficiently robust to provide a good fit for the results

obtained from the process at different conditions. Consequently, the model can be considered as a way to compress the information contained in the data so as to represent it in a more-readable and optimal way than the traditional one for correlative and predictive analysis purposes (see Section 1).

Finally, the fourth condition is connected to the fact that it is very difficult (if not impossible in practical and economic terms) to obtain in detail information on all the possible species of paraffins, olefins and aromatics, so as to close the carbon balance. This means that the total number of moles for each of these molecular systems will be an unknown from an empirical point of view (although, to date, good approximations have been obtained for the aromatics system [11]). Therefore, for paraffins and olefins, the total number of moles must be estimated based on predictions of a function that be consistent with the chemical characteristics of the evaluated process.

Additional Figures

Figs. A2, A3

Additional Tables

Table A1–A8

References

[1] R. Praveen Kumar, J. Kenthorai Raman, E. Gnansounou, G. Baskar, eds., Refining Biomass Residues for Sustainable Energy and Bioproducts, Elsevier, 2020. https://doi.org/10.1016/C2018-0-05005-7.

[2] Mandviwala C, Berdugo Vilches T, Seemann M, Faust R, Thunman H. Thermochemical conversion of polyethylene in a fluidized bed: Impact of transition metal-induced oxygen transport on product distribution. J Anal Appl Pyrolysis 2022;163:105476.

[3] Berdugo Vilches T, Marinkovic J, Seemann M, Thunman H. Comparing Active Bed Materials in a Dual Fluidized Bed Biomass Gasifier: Olivine, Bauxite, Quartz-Sand, and Ilmenite. Energy Fuel 2016;30:4848–57. https://doi.org/10.1021/acs.energyfuels.6b00327.

[4] Pecho J, Schildhauer TJ, Sturzenegger M, Biollaz S, Wokaun A. Reactive bed materials for improved biomass gasification in a circulating fluidised bed reactor. Chem Eng Sci 2008;63:2465–76. https://doi.org/10.1016/J.CES.2008.02.001.

[5] Weitkamp J. Catalytic Hydrocracking—Mechanisms and Versatility of the Process. ChemCatChem 2012;4:292–306. https://doi.org/10.1002/cctc.201100315.

[6] Mikulec J, Vrbova M. Catalytic and thermal cracking of selected polyolefins. Clean Technol Environ Policy 2008;10:121–30. https://doi.org/10.1007/s10098-007-0132-5.

[7] de Klerk A. Thermal Cracking of Fischer–Tropsch Waxes. Ind Eng Chem Res 2007;46:5516–21. https://doi.org/10.1021/ie070155g.

[8] Luo G, Suto T, Yasu S, Kato K. Catalytic degradation of high density polyethylene and polypropylene into liquid fuel in a powder-particle fluidized bed. Polym Degrad Stab 2000;70:97–102. https://doi.org/10.1016/S0141-3910(00)00095-1.

[9] Wang J, Jiang J, Wang X, Liu S, Shen X, Cao X, et al. Polyethylene upcycling to fuels: Narrowing the carbon number distribution in n-alkanes by tandem hydropyrolysis/hydrocracking. Chem Eng J 2022;444:136360. https://doi.org/10.1016/J.CEJ.2022.136360.

[10] Israelsson M, Seemann M, Thunman H. Assessment of the Solid-Phase Adsorption Method for Sampling Biomass-Derived Tar in Industrial Environments. Energy Fuel 2013;27:7569–78. https://doi.org/10.1021/ef401893j.

[11] Berdugo Vilches T, Seemann M, Thunman H. Influence of In-Bed Catalysis by Ash-Coated Olivine on Tar Formation in Steam Gasification of Biomass. Energy Fuel 2018;32:9592–604. https://doi.org/10.1021/acs.energyfuels.8b02153.

[12] Chakraborty S. Generating discrete analogues of continuous probability distributions-A survey of methods and constructions. J Stat Distrib Appl 2015;2:6. https://doi.org/10.1186/s40488-015-0028-6.

[13] Coles S. An Introduction to Statistical Modeling of Extreme Values, Springer, London. London 2001. https://doi.org/10.1007/978-1-4471-3675-0.

[14] Israelsson M, Larsson A, Thunman H. Online Measurement of Elemental Yields, Oxygen Transport, Condensable Compounds, and Heating Values in Gasification Systems. Energy Fuel 2014;28:5892–901. https://doi.org/10.1021/ef501433n.

[15] Berguerand N, Berdugo Vilches T. Alkali-Feldspar as a Catalyst for Biomass Gasification in a 2-MW Indirect Gasifier. Energy Fuel 2017;31:1583–92. https://doi.org/10.1021/acs.energyfuels.6b02312.

[16] J. Maric, Choice of bed material: a critical parameter in the optimization of dual fluidized bed systems, in: 2016.

[17] Faust R, Berdugo Vilches T, Malmberg P, Seemann M, Knutsson P. Comparison of Ash Layer Formation Mechanisms on Si-Containing Bed Material during Dual Fluidized Bed Gasification of Woody Biomass. Energy Fuel 2020;34:8340–52. https://doi.org/10.1021/acs.energyfuels.0c00509.

[18] W. Kaminsky, The Hamburg Fluidized-bed Pyrolysis Process to Recycle Polymer Wastes and Tires, in: Feedstock Recycling and Pyrolysis of Waste Plastics, John Wiley & Sons, Ltd, 2006: pp. 475–491. https://doi.org/https://doi.org/10.1002/0470021543.ch17.

[19] Levine SE, Broadbelt LJ. Detailed mechanistic modeling of high-density polyethylene pyrolysis: Low molecular weight product evolution. Polym Degrad Stab 2009;94:810–22. https://doi.org/10.1016/J.POLYMDEGRADSTAB.2009.01.031.

[20] Zhao D, Wang X, Miller JB, Huber GW. The Chemistry and Kinetics of Polyethylene Pyrolysis: A Process to Produce Fuels and Chemicals. ChemSusChem 2020;13:1764–74. https://doi.org/10.1002/cssc.201903434.

[21] T.B. Vilches, Operational strategies to control the gas composition in dual fluidized bed biomass gasifiers, in: 2018.